J|A|C|S ARTICLES

Published on Web 04/01/2009

Spontaneous Chiral Resolution in Supramolecular Assembly of 2,4,6-Tris(2-pyridyl)-1,3,5-triazine on Au(111)

Jing Zhang, Bin Li, Xuefeng Cui, Bing Wang,* Jinlong Yang, and J. G. Hou*

Hefei National Laboratory for Physical Sciences at Microscale, University of Science and Technology of China, Hefei, Anhui 230026, People's Republic of China

Received January 10, 2009; E-mail: bwang@ustc.edu.cn; jghou@ustc.edu.cn

Abstract: We have investigated the self-assembly of 2,4,6-tris(2-pyridyl)-1,3,5-triazine (TPTZ) molecule on Au(111) surface using an ultrahigh vacuum low-temperature scanning tunneling microscope. The TPTZ molecules form enantiomorphous domains composed of rhombic supercells with various periods depending on the coverage of molecules, that is, "1 × 1" and "2 × 2" structures at low coverages, and "6 × 6", "7 × 7", and "8 × 8" structures at higher coverages. In a unit cell of a certain enantiomer, the two triangular half-unit cells, consisting of adsorbed TPTZ molecules, are centrosymmetric to each other. The molecules inside each half-unit cell are bound to each other through a single −CH···N− hydrogen bond, while the molecules at the boundaries between half-unit cells are bound through double −CH···N− hydrogen bonds. The STM images and the DFT calculations reveal that the molecules in an enantiomorphous domain adopt the same adsorption orientation of either *R*-TPTZ or *L*-TPTZ, which indicates that the adsorbed TPTZ molecules on Au(111) undergo spontaneous chiral resolution. The subtle balance between the intermolecular interaction and the molecule−substrate interaction tunes the period of the superstructure. The total interaction energy densities obtained from the DFT calculations explain the experimental observations quantitatively.

Introduction

The control of chirality in synthetic supramolecular self-assembled two-dimensional (2D) systems becomes very important for designing electronic and optoelectronic devices at molecular scale,[1−5] as well as for understanding and applications of these systems, for example, in chiral molecular recognition[6] or mimicking biological functions.[7] The idea includes production of highly ordered supramolecular architectures and formation or isolation of ordered pure enantiomers. However, a supramolecular assembly usually occurs via noncovalent interactions, such as hydrogen bond (HB),[8−10] dipolar coupling,[11] and zwitterionic coupling.[4] Moreover, the subtle balance between the intermolecular interaction and the molecule−substrate interaction may cause the variation of the structures. For example, the trimesic acid (TMA) molecules form a serial of honeycomb motifs with various periods by varying of coverage,[12] molecular adsorption orientation,[13] or changing substrate.[14,15] These factors may interplay and cause the lower stability and the higher susceptibility to racemization in supramolecular assemblies.[16,17] The adsorption of molecules on solid surfaces restricts the molecules into two-dimensional objects, which may induce the molecular chirality due to asymmetric distortion of the molecular frame[18−20] or just because of losing mirror symmetry.[16,17,21] The chirality makes the structures possess more intriguing phenomena and potential applications in enantioselective heterogeneous catalysis.[21,22] Various chiral phenomena, such as chiral resolution,[17−20,23−30] chiral amplification,[31] and

(1) Meijer, E. W.; Schenning, A. *Nature (London)* **2002**, *419*, 353–354.
(2) Percec, V.; Glodde, M.; Bera, T. K.; Miura, Y.; Shiyanovskaya, I.; Singer, K. D.; Balagurusamy, V. S. K.; Heiney, P. A.; Schnell, I.; Rapp, A.; Spiess, H. W.; Hudson, S. D.; Duan, H. *Nature (London)* **2002**, *419*, 384–387.
(3) Barth, J. V.; Costantini, G.; Kern, K. *Nature (London)* **2005**, *437*, 671–679.
(4) Schiffrin, A.; Riemann, A.; Auwärter, W.; Pennec, Y.; Weber-Bargioni, A.; Cvetko, D.; Cossaro, A.; Morgante, A.; Barth, J. V. *Proc. Natl. Acad. Sci. U.S.A.* **2007**, *104*, 5279–5284.
(5) De Feyter, S.; De Schryver, F. C. *Chem. Soc. Rev.* **2003**, *32*, 139–150.
(6) Reinhoudt, D. N.; Crego-Calama, M. *Science* **2002**, *295*, 2403–2407.
(7) Fiammengo, R.; Crego-Calama, M.; Reinhoudt, D. N. *Curr. Opin. Chem. Biol.* **2001**, *5*, 660–673.
(8) Wang, Y. F.; Ge, X.; Schull, G.; Berndt, R.; Bornholdt, C.; Koehler, F.; Herges, R. *J. Am. Chem. Soc.* **2008**, *130*, 4218–4219.
(9) Yokoyama, T.; Yokoyama, S.; Kamikado, T.; Okuno, Y.; Mashiko, S. *Nature (London)* **2001**, *413*, 619–621.
(10) Meier, C.; Ziener, U.; Landfester, K.; Weihrich, P. *J. Phys. Chem. B* **2005**, *109*, 21015–21027.
(11) Baber, A. E.; Jensen, S. C.; Sykes, E. C. H. *J. Am. Chem. Soc.* **2007**, *129*, 6368–6369.
(12) Ye, Y. C.; Sun, W.; Wang, Y. F.; Shao, X.; Xu, X. G.; Cheng, F.; Li, J. L.; Wu, K. *J. Phys. Chem. C* **2007**, *111*, 10138–10141.
(13) Dmitriev, A.; Lin, N.; Weckesser, J.; Barth, J. V.; Kern, K. *J. Phys. Chem. B* **2002**, *106*, 6907–6912.
(14) Griessl, S.; Lackinger, M.; Edelwirth, M.; Hietschold, M.; Heckl, W. M. *Single Mol.* **2002**, *3*, 25–31.
(15) Sheerin, G.; Cafolla, A. A. *Surf. Sci.* **2005**, *577*, 211–219.
(16) Huang, T.; Hu, Z. P.; Wang, B.; Chen, L.; Zhao, A. D.; Wang, H. Q.; Hou, J. G. *J. Phys. Chem. B* **2007**, *111*, 6973–6977.
(17) Huang, T.; Hu, Z. P.; Zhao, A. D.; Wang, H. Q.; Wang, B.; Yang, J. L.; Hou, J. G. *J. Am. Chem. Soc.* **2007**, *129*, 3857–3862.
(18) Fasel, R.; Wider, J.; Quitmann, C.; Ernst, K.-H.; Greber, T. *Angew. Chem., Int. Ed.* **2004**, *43*, 2853–2856.
(19) Parschau, M.; Kampen, T.; Ernst, K.-H. *Chem. Phys. Lett.* **2005**, *407*, 433–437.
(20) Tao, F.; Bernasek, S. L. *J. Phys. Chem. B* **2005**, *109*, 6233–6238.
(21) France, C. B.; Parkinson, B. A. *J. Am. Chem. Soc.* **2003**, *125*, 12712–12713.
(22) Ortega Lorenzo, M.; Baddeley, C. J.; Muryn, C.; Raval, R. *Nature (London)* **2000**, *404*, 376–379.
(23) Stepanow, S.; Lin, N.; Vidal, F.; Landa, A.; Ruben, M.; Barth, J. V.; Kern, K. *Nano Lett.* **2005**, *5*, 901–904.

chiral phase transition,[32−34] have been observed in the 2D molecular systems. Despite such achievements, hitherto it still remains a challenging task to predict and control over the supramolecular chirality.

Here, we present a scanning tunneling microscopy (STM) study of the self-assembly of 2,4,6-tris(2-pyridyl)-1,3,5-triazine[35] (TPTZ) molecules on Au(111). The spontaneous chiral resolution occurs in superstructured assembly of TPTZ with tunable periods by adjusting the coverage of molecules. The chiral TPTZ molecules adsorbed on the Au(111) surface form a series of enantiomorphous superstructures with a rhombic unit cell composed of two centrosymmetric triangular half-unit cells. Combining the experimental observations with the density functional theory (DFT) calculations, we find that the enantiomorphous superstructures undergo spontaneous resolution upon the self-assembly of the TPTZ molecules, that is, each domain containing homochiral molecules due to the enantioselective interaction determined by the intermolecular interaction.

Experimental Section

All experiments were performed using a homemade low-temperature STM in a UHV chamber (base pressure $< 3 \times 10^{-8}$ Pa). Atomically flat Au(111) surface was prepared by vacuum evaporating Au film on mica and cleaning by repeated cycles of Ar^+ sputtering (800 eV) and annealing at 600 K for 30 min. The 2,4,6-tris(2-pyridyl)-1,3,5-triazine (TPTZ) molecules (97%, Aldrich) had been heated at 380 K with a Knudsen-cell type evaporator in vacuum for about 10 h to exile impurities before deposition. TPTZ samples were prepared by sublimation of TPTZ molecules with a typical deposition rate of about 0.06 ML/min at 370 K while the Au(111) substrate was kept at room temperature, where 1 ML is defined as a molecule density of 1.08 nm^{-2} according to the close packed TPTZ molecules. It was found that the TPTZ films always showed gas-like phase without ordered structure at room temperature. The situation was not changed by varying the deposition rate and heating the substrate temperature during molecule sublimation. The ordered structure of TPTZ assembly can be imaged only at low temperature. After deposition, the samples were transferred into the cryostat of the microscope and cooled to 120 K within 3 h. All of the STM images presented in this Article were acquired with a constant current mode at 120 K. An electrochemically etched tungsten tip was used.

Theoretical Methods. DFT-based calculations were performed using the molecular simulation DMol3 package.[36−38] The linear combination of atomic orbital and molecular orbital (LCAO-MO) method was adopted. The atomic orbitals were represented by a double-numeric quality basis set with d-polarization functions (DNP) and density functional semicore pseudopotential (DSPP) corrections.[39] At the local density approximation (LDA) level, we chose the Vosko−Wilk−Nusair (VWN) local correlation functional[40] using parametrizations of Ceperley and Alder's electron gas Monte Carlo data.[41] The electronic structure was obtained by solving the Kohn−Sham equations self-consistently in the spin-polarized scheme.

Considering that both the intermolecular interaction and the molecule−substrate interaction affect the self-assembled structure of TPTZ, we examined these two interactions by performing DFT calculations. The intermolecular interaction at the boundaries between triangular half-unit cells was calculated with a 2D single molecular layer based on a "1 × 1" structure, in which each half-unit cell contains one TPTZ molecule. The intermolecular interaction inside a half-unit cell was calculated with a 2D close packed structure of TPTZ. A vacuum layer of 15.0 Å between molecular layers was used for the both cases. Various configurations of molecules with different orientation, *R*-TPTZ or *L*-TPTZ, had been included. The Brillouin-zone integrations had been performed on a 2 × 2 × 1 Monkhorst-Pack grid of k-points for the first case of "1 × 1" structure and a 3 × 3 × 1 Monkhorst-Pack grid of k-points for the latter case of closed packed structure, which allows convergence to be reached for the calculated energy. Both the distance between molecules and the relative orientation in the molecular plane were optimized. The binding energy was obtained by subtracting the total energy of a single molecule in the gas phase from the total energy of a molecule in the assembled monolayer within unit of "1 × 1" structure. STM images were simulated by the Tersoff−Hamann formula.[42]

The molecule−substrate interaction was calculated on the basis of a (6 × 6) supercell of an Au(111) periodic three-layer slab model with a TPTZ molecule on one side of the slab. A vacuum layer of 20.0 Å was used to separate the slabs. The bulk Au−Au distance of 2.88 Å was used. Initial configurations of a TPTZ molecule on Au(111) were constructed by locating the central triazine ring at the top site (T), hcp hollow site (H_h), or fcc hollow site (H_f), with different orientations of the other three pyridine lobes. In the structural optimizations of different adsorption configurations, we fixed the Au atoms in the second and third layers and only allow the 36 Au atoms in the first layer and all atoms of the TPTZ molecule to relax. In each case, the full atomic relaxation was performed until the forces on atoms were smaller than 0.02 eV/Å. The Brillouin-zone integrations had been performed only on Γ-point for all structures.

Results and Discussion

There are two possible conformations for TPTZ named A and B conformations.[35,43] Conformation B has a lower energy than conformation A by 11.30 kJ/mol,[35,43] which is about 4 times greater than the thermal energy value of 2.5 kJ/mol at room temperature; thus conformation B is more preferred than conformation A at room temperature or lower temperatures. The TPTZ molecules with conformation B have a 3-fold symmetry axis. They become chiral upon adsorption because the substrate breaks mirror symmetry with respect to the molecular plane.[5,44]

(24) Fasel, R.; Parschau, M.; Ernst, K.-H. *Angew. Chem., Int. Ed.* **2003**, *42*, 5178–5181.
(25) Pérez-Garcı´a, L.; Amabilino, D. B. *Chem. Soc. Rev.* **2007**, *36*, 941–967.
(26) Wang, D.; Xu, Q. M.; Wan, L. J.; Bai, C. L.; Jin, G. *Langmuir* **2003**, *19*, 1958–1962.
(27) Weckesser, J.; De Vita, A.; Barth, J. V.; Cai, C.; Kern, K. *Phys. Rev. Lett.* **2001**, *87*, 096101.
(28) Böhringer, M.; Morgenstern, K.; Schneider, W.-D.; Berndt, R.; Mauri, F.; De Vita, A.; Car, R. *Phys. Rev. Lett.* **1999**, *83*, 324–327.
(29) Kühnle, A.; Linderoth, T. R.; Hammer, B.; Besenbacher, F. *Nature (London)* **2002**, *415*, 891–893.
(30) Chen, Q.; Richardson, N. V. *Nat. Mater.* **2003**, *2*, 324–328.
(31) Fasel, R.; Parschau, M.; Ernst, K.-H. *Nature (London)* **2006**, *439*, 449–452.
(32) Vidal, F.; Delvigne, E.; Stepanow, S.; Lin, N.; Barth, J. V.; Kern, K. *J. Am. Chem. Soc.* **2005**, *127*, 10101–10106.
(33) Böhringer, M.; Schneider, W.-D.; Berndt, R. *Angew. Chem., Int. Ed.* **2000**, *39*, 792–795.
(34) Romer, S.; Behzadi, B.; Fasel, R.; Ernst, K.-H. *Chem.-Eur. J.* **2005**, *11*, 4149–4154.
(35) Drew, M. G. B.; Hudson, M. J.; Iveson, P. B.; Russell, M. L.; Madic, C. *Acta Crystallogr., Sect. C.: Cryst. Struct. Commun.* **1998**, *54*, 985–987.
(36) Kohn, W.; Sham, L. J. *Phys. Rev.* **1965**, *140*, A1133−1138.
(37) Kohn, W.; Sham, L. J. *Phys. Rev.* **1966**, *145*, 561.
(38) Delley, B. *J. Chem. Phys.* **2000**, *113*, 7756.
(39) Hamann, D. R.; Schluter, M.; Chiang, C. *Phys. Rev. Lett.* **1979**, *43*, 1494–1497.
(40) Vosko, S. H.; Wilk, L.; Nusair, M. *Can. J. Phys.* **1980**, *58*, 1200–1211.
(41) Ceperley, D. M.; Alder, B. J. *Phys. Rev. Lett.* **1980**, *45*, 566–569.
(42) (a) Tersoff, J.; Hamann, D. R. *Phys. Rev. Lett.* **1983**, *50*, 1998–2001. (b) Tersoff, J.; Hamann, D. R. *Phys. Rev. B* **1985**, *31*, 805–813.
(43) Janczak, J.; Śledź, M.; Kubiak, R. *J. Mol. Struct.* **2003**, *659*, 71–79.
(44) Barlow, S. M.; Raval, R. *Surf. Sci. Rep.* **2003**, *50*, 201–341.

Scheme 1. Schematic Model of Chiral *R*-TPTZ and *L*-TPTZ Molecules

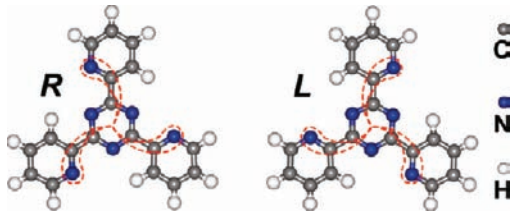

According to their adsorption orientations, the TPTZ molecules can be divided into *R*-TPTZ and *L*-TPTZ (Scheme 1), in which the N atoms of the pyridine rings adopt the relative positions counterclockwise and clockwise, respectively.

Figure 1a shows an STM image of TPTZ assembly with a density of molecules of 0.88 ± 0.04 nm^{-2}. All of the molecules nearly give the equivalent "Y" shape in the images, indicating that the molecules adopt a flat-lying adsorption. TPTZ molecules form ordered honeycomb-like superstructure. In this structure, each unit cell contains two TPTZ molecules, as marked by the diamonds in Figure 1a. The lattice constant (pore-to-pore distance) is about 1.62 ± 0.04 nm. We denote this structure as "1×1" according to the number of molecules along one lateral side of the unit cell. It is found that the "1×1" structure is incommensurate to the gold lattice, and the angle, α, between the lattice vector of the TPTZ superstructure and the $[11\bar{2}]$ direction of the gold substrate is in the range of $3-19°$ with a

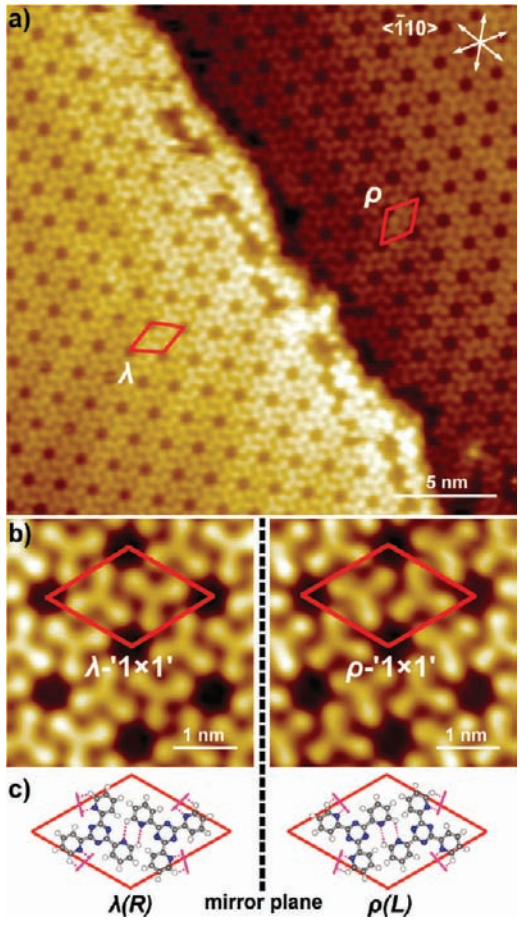

Figure 1. (a) STM image of TPTZ assembly with "1×1" structure on Au(111), $V_{bias} = 1.4$ V, $I_{set} = 0.2$ nA, measured at 120 K. (b) Magnified images of λ-"1×1" and ρ-"1×1" phases. (c) Schematic models of the most energetically favored configurations of the TPTZ molecules.

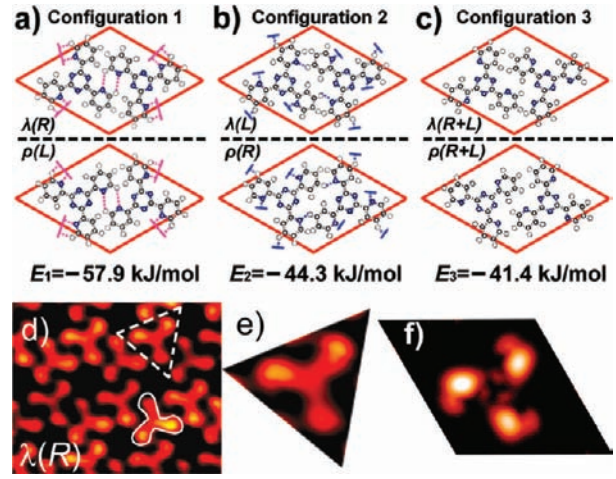

Figure 2. Possible configurations of chiral molecules upon adsorption with (a), (b) pure *R*-TPTZ or *L*-TPTZ in a unit cell for λ and ρ phases, respectively, and (c) mixture of one *R*-TPTZ and one *L*-TPTZ in a unit cell. The $-CH\cdots N-$ hydrogen bonds were marked with dashed lines. The calculated interaction energies per molecule are obtained by $E_i = (E_{total} - 2E_{free\text{-}TPTZ})/2$, where $i = 1$, 2, and 3, denoting three different configurations, E_{total} is the calculated total energy of a unit cell, and $E_{free\text{-}TPTZ}$ is the energy of a free TPTZ molecule in gas phase. (d) High contrast STM images ($V_{bias} = 1.4$ V and $I_{set} = 0.2$ nA, measured at 120 K), and (e) magnified image of a molecule marked by the dashed triangle in (d). (f) Simulated image of a *R*-TPTZ molecule on Au(111) with a sample bias of 1.5 V at a constant height of 3 Å.

Gaussian distribution. The angle α also reflects the orientation of the TPTZ molecules because one of the pyridine rings is almost parallel to the lattice vector in all of the superstructures. The molecule density of the "1×1" superstructure seems to be a threshold value in obtaining an ordered assembly. When the deposited molecules have a coverage lower than the threshold value, the TPTZ film exhibits a gas-like phase even at 120 K (see the STM image in the Supporting Information).

Interestingly, the TPTZ assembled monolayer contains two mirror-imaged 2D chiral domains, that is, enantiomorphous phases, denoted as λ and ρ phases (see magnified images in Figure 1b), respectively. It is found that the chirality and the superstructure of the TPTZ monolayer may be conserved across $\langle\bar{1}10\rangle$ steps of Au(111), but may be randomly performed on different terraces. According to the orientations of the molecules, there are three pairs of possible configurations in each unit cell of "1×1" structure, as shown in Figure 2. We performed DFT calculations with a 2D crystal, that is, a single molecular layer based on these "1×1" structures. The effect of the substrate is not included temporarily. The calculations revealed that the enantiomorphous domains of configuration **1**, that is, each unit cell contains the pure enantiomers with either *R*-TPTZ in λ phase [denoted as $\lambda(R)$] or *L*-TPTZ in ρ phase [denoted as $\rho(L)$] (Figure 2a), have the same interaction energy per molecule, $E_1 = -57.9$ kJ/mol. In this configuration, each molecule interacts with three other molecules, which can be mainly attributed to three double hydrogen bonds of $-CH\cdots N-$; thus each double hydrogen bond has an interaction energy of -19.3 kJ/mol, which is consistent with the values reported before.[9,10] Even though the molecules adopt pure enantiomers in configuration **2** (Figure 2b), the interaction energies per molecule become larger by 13.6 kJ/mol than those for configuration **1**. The energy values for the mixture configuration **3** are quite similar to those for configuration **2**. Our calculations show that pure enantiomers of $\lambda(R)$ and $\rho(L)$ have the lowest intermolecular interaction energy per molecule, suggesting that the enantiomorphous

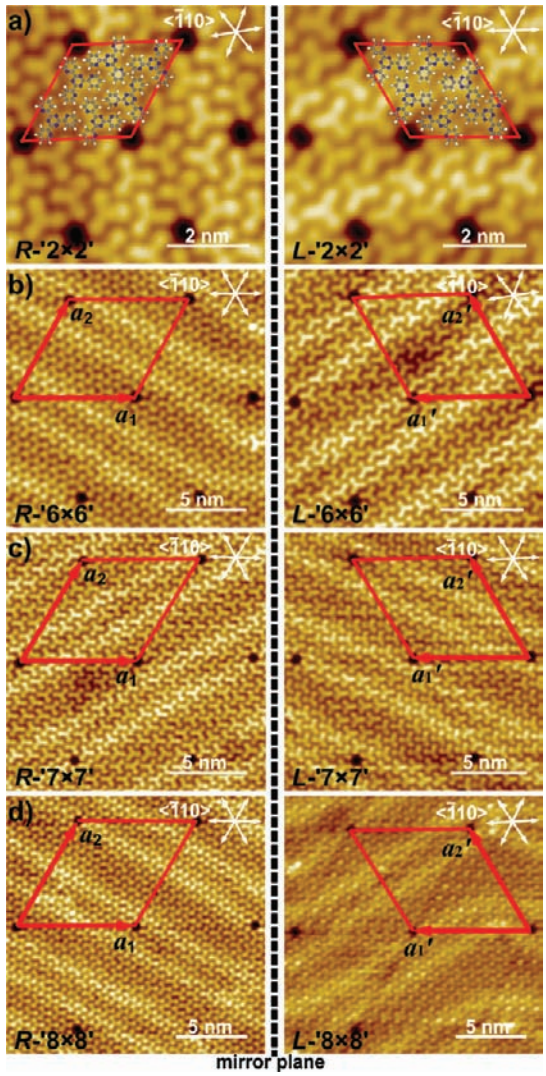

Figure 3. STM images (V_{bias} = 1.4 V and I_{set} = 0.2 nA, measured at 120 K) of TPTZ enantiomorphous domains of (a) "2 × 2", (b) "6 × 6", (c) "7 × 7", and (d) "8 × 8" superstructures.

domain of $\lambda(R)$ [or $\rho(L)$] is composed of homochiral molecules of *R*-TPTZ (or *L*-TPTZ). The high contrast STM image and the simulated image confirm the conclusion. As shown in Figure 2d, the three pyridine rings in each TPTZ molecule exhibit distortion. As indicated by the contours, the distorted tail at each pyridine ring uniformly orientates counterclockwise in λ phase. One of the molecules is magnified in Figure 2e and compared to the simulated image of a *R*-TPTZ molecule on Au(111) in Figure 2f. The distorted tail at each pyridine ring may be attributed to the N atoms of the pyridine rings (Scheme 1). A similar result is obtained for *L*-TPTZ molecules. Thus, the uniform orientations of molecules in λ and ρ phases, respectively, reflect their homochiralities.

With increasing densities of molecules, the TPTZ assemblies exhibit either λ-"$n \times n$" or ρ-"$n \times n$" phases with superstructure order n = 2, 6, 7, and 8 (Figure 3). Here, n denotes the molecule number along a lateral side of the unit cell. In our experiment, the superstructures with n = 3, 4, and 5 were only observed sparsely and imperfectly between domains of other structures or defected areas. The superstructures with higher orders ($n \geq 9$) were seldom observed. In all of the observed superstructures, the molecules at boundaries between half-unit cells form DHBs of −CH···N−, similar to the case of the "1 × 1" structure, while inside half-unit cells the molecules are close packed (see the superposed molecules in Figure 3a). Much higher densities of molecules led to growth of the second layer, while the first layer tended to be close packed.

The intermolecular interaction inside half-units may be different from that at half-unit boundaries. As shown in Figure 4, 2D close-packed structures were used to simulate the interaction between the close-packed molecules inside the same half-unit cell. In the calculations, we considered the assemblies of pure *R*-TPTZ (or *L*-TPTZ) molecules (Figure 4a) and a mixture of *R*-TPTZ and *L*-TPTZ molecules with various ratios of 3:1 (Figure 4b) and 1:1 (Figure 4c), respectively. The calculations gave the average interaction energies per molecule, E_{homo} = −51.0 kJ/mol, $E_{hetero\text{-}3:1}$ = −30.1 kJ/mol, and $E_{hetero\text{-}1:1}$ = −27.4 kJ/mol, for these three assemblies. The racemic mixture (with ratio of 1:1) has the highest interaction energy per molecule. The interaction energies per molecule for mixtures tend to decrease with more and more deviation from the racemic mixture; for example, the value for the ratio of 3:1 (or 1:3) changes to −30.1 kJ/mol. The results indicate that the assemblies with pure enantiomers of *R*-TPTZ (or *L*-TPTZ) are most energetically favorable; thus the molecules inside the same half-unit cell tend to assemble with homochirality, which may form trimeric hydrogen bonds of −CH···N− (Figure 4a), similar to the cases of trimesic acid (TMA),[12] 1,3,5-benzenetribenzoic acid,[14,45] and hexaphenylbenzene (HPB).[46] The intermolecular interactions both at boundaries and inside half-unit cells lead to homochiral assembly of $\lambda(R)$ or $\rho(L)$ domains. Hence, we may conclude that the spontaneous chiral separation observed in TPTZ assemblies is driven by the intermolecular interactions mainly comprising the double hydrogen bonds and trimeric hydrogen bonds.

The parameters for the observed supramolecular superstructures are summarized in Table 1. It is noted that "2 × 2" structure, similar to "1 × 1" structure, is incommensurate to the Au(111) substrate, and α varies in the range of 7−22° with Gaussian distribution. In the cases of n = 6, 7, and 8, the α values vary in a narrow range, and the periods of the superstructures are almost integral multiple to the lattice period of the Au(111) substrate, indicating that the TPTZ assemblies become commensurate to the gold substrate. In these cases, the interactions between the molecules and the substrate become not negligible. Xiao et al.[46] proposed that a C_3 symmetric molecule will be able to self-assemble into a series of higher order honeycomb network structures if the molecule can form both a honeycomb network via a strong and directional binding and a hexagonal close-packed structure via a weaker interaction. However, in those works, the interactions between the molecule and the substrate were not considered.

To evaluate the effect of the substrate on the adsorption of TPTZ molecules, we calculated the adsorption configurations and energies of TPTZ on the Au(111) surface. For simplicity, we only considered a single TPTZ molecule on Au(111). This treatment makes it possible to implement the calculations, dealing with a large number of atoms when we take the effect of substrate into account. After the structural optimization, we obtained 12 stable configurations. The adsorption configurations are labeled as T_m, H_{hm}, and H_{fm}, where T denotes top site

(45) Ruben, M.; Payer, D.; Landa, A.; Comisso, A.; Gattinoni, C.; Lin, N.; Collin, J. P.; Sauvage, J. P.; De Vita, A.; Kern, K. *J. Am. Chem. Soc.* **2006**, *128*, 15644–15651.
(46) Xiao, W. D.; Feng, X. L.; Ruffieux, P.; Gröning, O.; Müllen, K.; Fasel, R. *J. Am. Chem. Soc.* **2008**, *130*, 8910–8912.

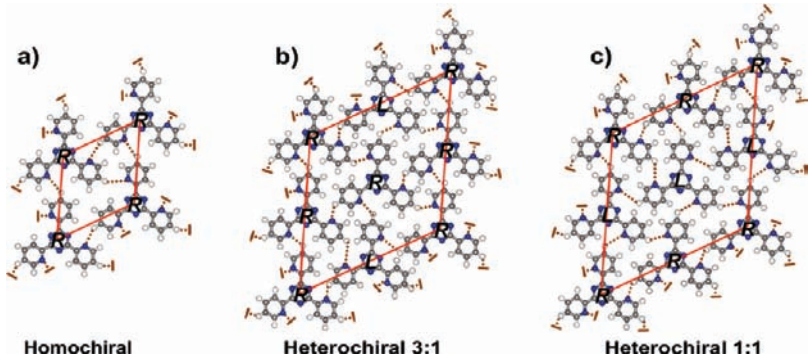

Figure 4. Schematic close-packed models used in calculations with (a) pure enantiomers by a 1 × 1 cell, (b) mixture with 3:1 ratio by a 2 × 2 cell, and (c) racemic mixture by a 2 × 2 cell. Average interaction energies per molecule are obtained by $E_{homo} = E_{total} - E_{free\text{-}TPTZ}$, $E_{hetero\text{-}3:1} = (E_{total} - 4E_{free\text{-}TPTZ})/4$, and $E_{hetero\text{-}1:1} = (E_{total} - 4E_{free\text{-}TPTZ})/4$.

Table 1. Parameters for Various Superstructures

	"1 × 1"	"2 × 2"	"6 × 6"	"7 × 7"	"8 × 8"
density of molecules (nm^{-2})	0.88 ± 0.04	0.95 ± 0.03	0.96 ± 0.02	0.98 ± 0.02	0.96 ± 0.01
α	3−19°	7−22°	26.2 ± 0.9°	28.7 ± 0.7°	29.2 ± 0.6°
a_{exp} (nm)	1.62 ± 0.04	2.70 ± 0.04	7.11 ± 0.08	8.14 ± 0.09	9.31 ± 0.05
a_{model} (nm)			7.35	8.50	9.65

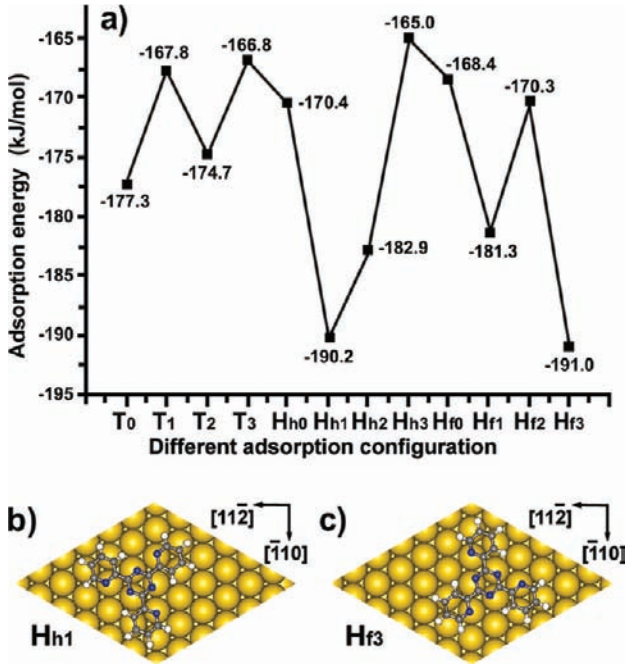

Figure 5. (a) Dependence of calculated adsorption energy per molecule on different adsorption configurations. (b and c) Two adsorption configurations of H_{h1} and H_{f3} with minimum adsorption energies.

adsorption of the molecular triazine center, H_h denotes hcp hollow site, H_f denotes fcc hollow site, and the subscription number m denotes the molecular orientation tilting clockwise (for *R*-TPTZ) or counterclockwise (for *L*-TPTZ) from the [11$\bar{2}$] direction of Au(111) by angle of $m \times 30°$ ($m = 0$, 1, 2, and 3), with $m = 0$ being defined as one pyridine lobe of the molecule along the [11$\bar{2}$] direction of Au(111) surface. The adsorption energy dependence on adsorption configuration for *R*-TPTZ is given in Figure 5. It is found that the H_{h1} and H_{f3} configurations are the most energetically preferred adsorption configurations (Figure 5b and c), with adsorption energies of −190.2 and −191.0 kJ/mol per molecule, respectively. A similar result is obtained for *L*-TPTZ adsorption. Here, we assume that the commensurate superstructures for $n \geq 6$ should adopt the H_{h1} and H_{f3} adsorption configurations, while the superstructures for $n \leq 5$ may deviate from such configurations, more or less.

According to the STM observations and the minimum energy configurations of H_{h1} and H_{f3}, we construct the structural models of λ-"$n \times n$" and ρ-"$n \times n$" (for example, λ-"6 × 6" is given in the Supporting Information). The molecules are adsorbed on the Au(111) surface with the central triazine ring on fcc hollow site and the three pyridine rings on hcp hollow site in one half-unit cell, and for the opposite half-unit cell the central triazine ring on hcp hollow site and the three pyridine rings on fcc hollow site. In these structural models, the reconstruction of Au(111) surface is not considered. With the models, the lattice constants a_{model} (pore-to-pore distance) are computed according to the Au(111) lattice and compared to experimental values a_{exp} (Table 1). Considering that the herringbone reconstruction of Au(111) surface compresses lattice by 4.4%,[11,47,48] we find that the values obtained from the models are correspondingly in good agreement with the experimental ones.

In the analysis above, it is now clear how the intermolecular interaction and the molecule−substrate interaction separately affect the chirality and the assembly of TPTZ molecules. However, it remains unclear on the absence of certain superstructure orders in STM observations. For a comprehensive understanding, we should quantitatively consider the interactions together. On the basis of the calculations for the intermolecular interaction, the intermolecular interaction energy per molecule is given by $E_{intermol}(n) = [2nE_1 + n(n-1)E_{homo}]/[n(n+1)]$. Here, we assumed that the intermolecular interaction energy per molecule at boundaries in superstructures of order $n \geq 2$ remains as the one, E_1, in "1 × 1" structure, and the intermolecular interaction energy per molecule inside half-unit cells, E_{homo}, remains unchanged. The molecule−substrate interaction energy per molecule was obtained by adopting the average value of the H_{h1} and H_{f3} configurations, which is only

(47) Wöll, C.; Chiang, S.; Wilson, R. J.; Lippel, P. H. *Phys. Rev. B* **1989**, *39*, 7988–7991.
(48) Barth, J. V.; Brune, H.; Ertl, G.; Behm, R. J. *Phys. Rev. B* **1990**, *42*, 9307–9318.

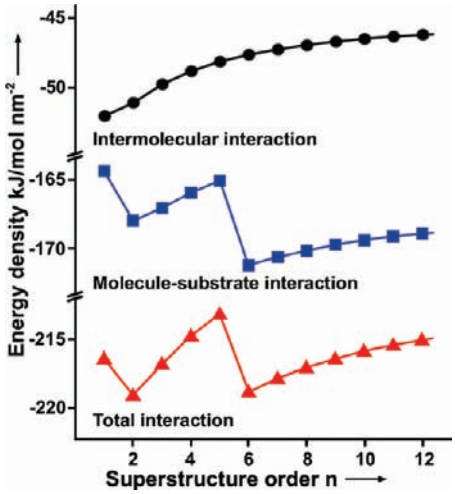

Figure 6. Interaction energy density as a function superstructure order n. ●: Intermolecular interaction energy density. ■: Molecule−substrate interaction energy density. ▲: Total interaction energy density. The lines are guides for the eyes.

valid for the commensurate superstructures with $n \geq 6$. Because the lower order superstructures (with $n = 1, 2$) are incommensurate to the Au substrate, it is difficult to calculate precisely the molecule−substrate interaction due to lack of exact adsorption configuration. Considering the variation of α is less than 30° deviated from the commensurate ones (Table 1), we adopt the interaction energy value of −182.9 kJ/mol for H_{h2} as the molecule−substrate interaction energy for $n \leq 5$. The exact value may be varied in a certain range depending on the actual adsorption configuration and the superstructure order n; however, the variation should be small based on our observations. The direct summation over the intermolecular interaction energy per molecule and the molecule−substrate interaction energy per molecule is still not sufficient to explain our experimental results (Supporting Information), because the interaction energy per molecule might not be sufficient to determine energy minimum configurations of 2D molecular systems.[46]

Instead, considering Kitaigorodskii's principle of close packing,[49] the analysis in terms of interaction energy densities, that is, interaction energy per unit area, may provide better understanding of our experimental observations. In Figure 6, the total interaction energy densities, obtained by summation of the intermolecular interaction energy densities and the molecule−substrate interaction energy densities, are plotted as a function of order n. The existence of two minimum energy densities for $n = 2$ and $n = 6$ well rationalizes the following experimental phenomena: (i) the observation of superstructures with $n = 1$, 2, 6, 7, 8 and coexistence of them; (ii) the rareness of superstructures with $n = 3$, 4, and 5; and (iii) the superstructures with $n = 2$ and 6 are observed more frequently than other superstructures.

As an extended discussion, we further consider the dynamic process in self-assembly of TPTZ superstructures. At room temperature, we only observed the gas-like phase of TPTZ films from submonolayer to 2 ML, indicating that the molecules are movable at room temperature. It means that the crystallization of TPTZ films can only be reached at a low temperature. During cooling to 120 K, the TPTZ assemblies relaxed and reached their energetically favorable structures. The ordered structures disappeared when we warmed the sample to room temperature. We have circularly cooled and warmed the samples with various coverages. The distributions of the superstructure orders measured at 120 K were statistically unchanged. Thus, the coexistent superstructures reflect the characteristic of the TPTZ assemblies at thermodynamic equilibrium.

It seems that there also exists a critical coverage to form the ordered structures. With TPTZ coverages lower than 0.6 ML, only the gas-like phase was observed without any ordered structure. When the coverage reached 0.7 ML, ordered "1 × 1" islands surrounded by a gas-like phase were observed (Supporting Information). So the coverage of molecules plays an important role in forming the ordered assemblies. Here, we argue that there exists a competition between intermolecular repulsion and attraction. At lower coverages, the repulsion is dominant, thus preventing the assembly of ordered structure. When the coverage reaches the critical one, the molecules are pushed close enough, so that the hydrogen-bond interaction becomes dominant. The overall repulsion increases with increasing the TPTZ coverage, while the hydrogen-bond interaction balances it in a certain range. The intermolecular interaction curve in Figure 6 energetically describes this process. Simultaneously, the molecule−substrate interaction as another factor interplays. However, the lattice mismatch between the TPTZ assembly and the Au substrate becomes a constraint for the energetically unfavorable superstructures, say, for $n = 3$, 4, and 5. Until the lattices match each other for higher order superstructures for $n \geq 6$, the system energy thus drops.

Conclusion

In summary, we accomplished the STM measurement of self-assemblies of TPTZ on Au(111) surface and the DFT calculation. A series of enantiomorphous superstructures with tunable period are formed by TPTZ molecules through the −CH···N− hydrogen bond. The intermolecular interaction induces the chiral resolution, forming TPTZ enantiomorphous superstructures. The competition between the intermolecular interaction and the molecule−substrate interaction tunes up the superstructure order. The presented analysis may be applicable to other supramolecular chiral systems.

Acknowledgment. This work was supported by NSFC (50721091, 10825415, 60771006, 50532040, 10704069) and NBRP (2006CB922001), China.

Supporting Information Available: Proposed structural model for λ-"6 × 6" superstructure, interaction energy per molecule as the function order n of the superstructures, coexistence of superstructures with different order n, and STM images for a nominal TPTZ coverage of 0.7 and 1.1 ML. This material is available free of charge via the Internet at http://pubs.acs.org.

JA9001986

(49) Kitaigorodsky, A. I. *Molecular Crystals and Molecules*; Academic Press: New York, 1973.